

PCCP

Accepted Manuscript



This is an *Accepted Manuscript*, which has been through the Royal Society of Chemistry peer review process and has been accepted for publication.

Accepted Manuscripts are published online shortly after acceptance, before technical editing, formatting and proof reading. Using this free service, authors can make their results available to the community, in citable form, before we publish the edited article. We will replace this *Accepted Manuscript* with the edited and formatted *Advance Article* as soon as it is available.

You can find more information about *Accepted Manuscripts* in the [Information for Authors](#).

Please note that technical editing may introduce minor changes to the text and/or graphics, which may alter content. The journal's standard [Terms & Conditions](#) and the [Ethical guidelines](#) still apply. In no event shall the Royal Society of Chemistry be held responsible for any errors or omissions in this *Accepted Manuscript* or any consequences arising from the use of any information it contains.

Elucidating the Conformational Energetics of Glucose and Cellobiose in Ionic Liquids

Vivek S. Bharadwaj[‡], Timothy C. Schutt[‡], Timothy C. Ashurst[‡], and C. Mark Maupin^{‡}*

[‡]Chemical and Biological Engineering Department, Colorado School of Mines, 1500 Illinois Street, Golden, CO 80401

Corresponding Author

* To whom correspondence should be addressed: CMM, email: cmmaupin@mines.edu, PHONE: 303-273-3197, FAX: 303-273-3730

Funding Sources

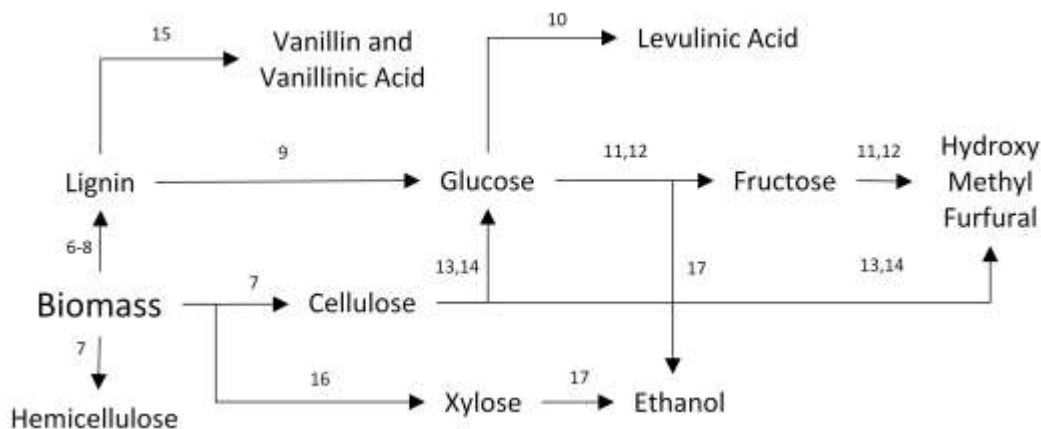
National Science Foundation (NSF Grant: CBET-1337044)

KEYWORDS: 1-Ethyl-3-Methylimidazolium Acetate (EMIM OAc), 1-Butyl-3-Methylimidazolium Acetate (BMIM OAc), 1-Ethyl-3-Octylimidazolium Acetate (OMIM OAc), Cellulose solvation, Metadynamics, Umbrella Sampling.

ABSTRACT: A major challenge for the utilization of lignocellulosic feedstocks for liquid fuels and other value added chemicals has been the recalcitrant nature of crystalline cellulose to various hydrolysis techniques. Ionic liquids (ILs) are considered to be a promising solvent for the dissolution and conversion of cellulose to simple sugars, which has the potential to facilitate the unlocking of biomass as a supplement and/or replacement for petroleum as a feedstock. Recent studies have revealed that the orientation of the hydroxymethyl group, described *via* the ω dihedral, and the glycosidic bond, described *via* the ϕ - ψ dihedrals, are significantly modified in the presence of ILs. In this study, we explore the energetics driving the orientational preference of the ω dihedral and the ϕ - ψ dihedrals for glucose and cellobiose in water and three imidazolium based ILs. It is found that interactions between the cation and the ring oxygen in glucose directly impact the conformational preference of the ω dihedral shifting the distribution towards the Gauche-Trans (GT) conformation and creating an increasingly unfavorable Gauche-Gauche (GG) conformation with increasing tail length. This discovery modifies the current hypothesis that intramolecular hydrogen bonding is responsible for the shift in the ω dihedral distribution and illuminates the importance of the cation's character. In addition, it is found that the IL's interaction with the glycosidic bond results in the modification of the observed ϕ - ψ dihedrals, which may have implications for hydrolysis in the presence of ILs. The molecular level information gained from this study identifies the favorable IL-sugar interactions that need to be exploited in order to enhance the utilization of lignocellulosic biomass as a ubiquitous feedstock.

1. Introduction

The recalcitrance of crystalline cellulose is a major obstacle hindering the immense potential of lignocellulosic biomass to supplement and possibly replace petroleum as a major feedstock. The kinetics of cellulose hydrolysis by both chemical and bio-chemical/enzymatic methods has been significantly limited due to the crystalline nature of cellulose. To some extent this recalcitrance issue has been overcome by the utilization of various pre-treatment techniques, one of the most promising of which has been ionic liquid pretreatment.¹⁻³ Ionic liquids (ILs) are a unique class of solvents that are salts in a liquid state at room temperature.⁴ They are promising candidates as replacements for volatile organic solvents since they have negligible vapor pressure, are non-flammable, and have relatively high thermal stability.⁴ ILs are highly versatile and may be tailored for specific tasks by varying the core ionic molecule and/or attached functional groups. Amongst the various multitude of ILs, the imidazolium based chlorides and acetates have proven to be some of the most effective at dissolving crystalline cellulose.¹ The main advantage of using imidazolium based ionic liquids has been their ability to not only dissolve crystalline cellulose, but also facilitate its conversion to value added products such as hydroxymethyl furfural (HMF) and total reducing sugars (*e.g.*, glucose, fructose, lactose and maltose).^{3, 5} Scheme 1 illustrates a few of the processes in which ionic liquids play a key role as solvents and reaction media, and aid in the conversion of biomass to various value added products.⁶⁻¹⁷ The significance of understanding how ILs solvate cellulose and its components is important considering the widespread involvement of ILs in various processes converting biomass to value added products.



Scheme 1: Processes that involve ILs as solvents to derive value added products from biomass with relevant literature noted along the corresponding arrows.

While there have been significant efforts to develop an efficient and cost effective process for the conversion of oligosaccharides to value added products, they rely on enzymes that function in an aqueous environment, in which oligosaccharides have limited solubility, or inorganic catalysts composed of expensive transition metals.¹⁸ In order to realize the most efficient route to utilize lignocellulosic biomass we must develop solvents that dissolve and facilitate the conversion of cellulose to total reducing sugars, all in a single reactor.¹⁹ This requires ILs that are compatible with not only process equipment, but are also benign towards and maintain, if not enhance, the efficacy of the catalysts (*e.g.*, cellobiohydrolase enzymes, metal chlorides).¹⁹ In this respect, the imidazolium acetate based ILs have shown significant promise.^{20, 21} Imidazolium based ionic liquids are characterized by a positively charged imidazolium ring that is flanked by a methyl group on one side and a longer, typically, hydrophobic alkyl group (*e.g.*, ethyl, butyl, or octyl) on the other side. Techniques such as Molecular Dynamics (MD) simulations have proven to be a powerful tool in revealing molecular level insights into the interactions between ILs, cellulose, and co-solvents.²²⁻²⁷ In regards to the interactions between ILs and cellulose, it has been

demonstrated that ILs can impact the conformational flexibility of microfibril cellulose and its constituent components, however, the energetics that govern this modified conformational flexibility in the presence of ILs is yet to be elucidated. One of the major factors that have impeded the evaluation of the energetics is the inherently viscous nature of pure ILs, which restricts conformational sampling of these systems. In a recent study, it has been observed that the presence of a co-solvent can play an important role in modulating the viscous nature of the IL without compromising the beneficial properties of the parent IL.²⁷

Currently the most popular ILs with regards to cellulose solvation have been 1-ethyl-3-methylimidazolium acetate (EMIM OAc) and 1-butyl-3-methylimidazolium chloride (BMIM Cl).^{1, 2, 28} While the behavior of cellulose and its representative polysaccharides in EMIM OAc has been explored,^{23, 25, 26} the impact of varying the cation's alkyl chain length on the underlying energetics has thus far not been evaluated. Furthermore, while the interactions of the poly or oligosaccharides have been studied,^{23, 25} specific interactions of glucose and cellobiose are as of yet unexplored. This study characterizes the specific interactions of alkyl imidazolium ILs with the constituent components of cellulose, namely glucose and cellobiose, and evaluates the impact of the cation's alkyl chain length on the solvation and conformational perturbation of glucose and cellobiose. We compare glucose and cellobiose solvation in an aqueous environment to the solvation characteristics of 3 ILs, 1-ethyl-3-methylimidazolium acetate (EMIM OAc), 1-butyl-3-methylimidazolium acetate (BMIM OAc) and 1-ethyl-3-octylimidazolium acetate (OMIM OAc). The MD simulations presented here provide structural insights, elucidate the energetics governing the conformations of glucose and cellobiose, and reveal the role played by the cation in driving conformational preference of sugars in ILs.

2. Methods

2.1 System Setup. All MD simulations used Amber12, were analyzed with AmberTools12, and utilized the PLUMED software packages for biased simulations.^{29, 30} The systems consisted of a glucose or cellobiose molecule in either water (7,653 water molecules), EMIM OAc (810 ion pairs), BMIM OAc (695 ion pairs) or OMIM OAc (542 ion pairs) constituting a total of 8 systems. The Glycam06 force field was used for glucose and cellobiose, TIP3P for water and an improved OPLS force field for the ILs.³¹⁻³³ The Packmol program was used to create the starting MD configurations, which were subsequently minimized for 4000 steps with the conjugated gradient algorithm followed by a cycling protocol.³⁴ The cycling protocol involved alternate equilibrations in the isobaric-isothermal (NPT) ensemble at 300 K and 1 atm for 500 ps, and the isochoric-isothermal (NVT) ensemble at 400 K for up to 5 ns. The cycling protocol was repeated until the system density was within 3% of the reported experimental density at 300 K. The various simulations were conducted with the hydrogen atoms restrained using the SHAKE algorithm and a 2 fs time step.³⁵ After the cycling simulations were completed, 10 ns of equilibration in the NVT ensemble at 300 K was performed followed by a 100 ns production run in the NVT ensemble at 300 K. After the production run was completed an additional 20 ns simulation was conducted in the microcanonical ensemble (NVE) at 300 K for computing the self-diffusivity coefficients.

2.2 Umbrella sampling. The solvation of glucose has been characterized by the conformational orientation of the hydroxymethyl group of glucose that is described *via* the ' ω ' (omega) dihedral angle (O6-C6-C5-O5), see Figure 1.³⁶ The biased umbrella sampling technique along with the weighted histogram analysis method (WHAM) was utilized for the construction of Potentials of

Mean Force (PMFs) describing the rotation around the ω angle in water and in each of the 3 ILs.³⁷⁻³⁹ Comparison of the PMFs for this dihedral rotation in water and the different ILs has enabled the evaluation of the impact of ILs on modifying the ω dihedral energy landscape. The restraining potential used was of the form,

$$U_n^{\text{umbrella sampling}}(x_{\text{dihedral}}) = \frac{k_n}{2}(x_{\text{dihedral}} - x_0^n)^2 \quad (1)$$

where $U_n^{\text{umbrella sampling}}$ is the restraining potential, k_n is the force constant, ξ_0 is the equilibrium dihedral angle for each window, and x_{dihedral} is the instantaneous value of the dihedral angle. For each system 37 windows spaced every 10° between -180° to 180° was conducted in the presence of a restraining potential force constant of $30 \text{ kcal/mol}\cdot\text{rad}^2$. Each window was equilibrated for 500 ps followed by a production run of 8 ns for the IL systems and 4 ns for the water systems. As with the unbiased simulations, the hydrogen atoms were restrained using the SHAKE algorithm and a 2 fs time step was employed. Convergence of the PMFs was evaluated by comparing PMFs calculated using the first half and last half of the simulation data. The final PMFs were considered converged when the standard deviation dropped below 0.3 kcal/mol (Supporting Information Figure S1).

2.2 Metadynamics simulations. Metadynamics has been an effective method for exploring complex free energy surfaces (FESs) over two or more dimensions⁴⁰⁻⁴³ and was thus chosen for elucidating the FES governing the phi (ϕ O5-C1-O4-C4) – psi (ψ C1-O4-C4-C5) dihedral conformation for the glycosidic bond in cellobiose. A biasing potential was applied on the collective variables phi (ϕ) and psi (ψ), and was of the form

$$V(s, t) = \sum_{k_\tau < t} W(k_\tau) \exp\left(\sum_{i=1}^d \frac{(s_i - s_i(q(k_\tau)))^2}{2\sigma_i^2}\right) \quad (2)$$

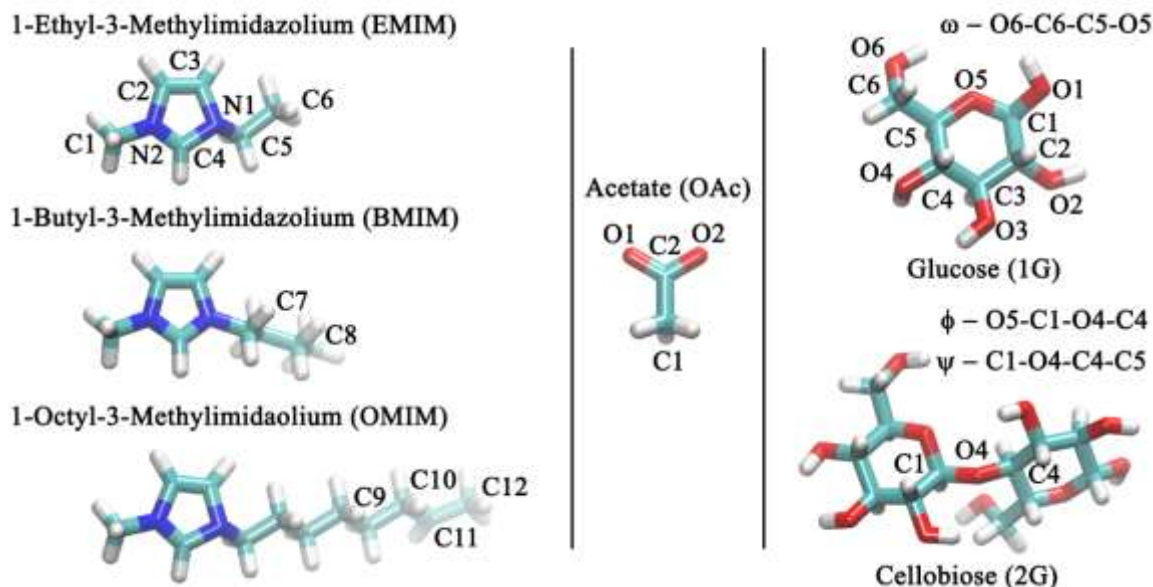


Figure 1 Structures of the cations, anion, and solute molecules

where V is the biasing potential, s is the collective variable, τ is the deposition rate between Gaussian additions, $W(k_\tau)$ is the height of the Gaussian, and σ_i is the Gaussian width. In well-tempered metadynamics (WTMD), the Gaussian height is re-scaled during the simulation according to a bias factor that allows for faster convergence times since large Gaussian heights are applied when the simulation visits an unsampled region and smaller Gaussian heights are used when the simulation revisits a previously sampled region.⁴⁴

The equilibrated cellobiose systems from the unbiased simulations were used as the starting points for the WTMD simulations that were conducted using Amber12 compiled with the PLUMED package.^{30, 44} For the WTMD simulations, a maximum hill height of 0.15 kcal/mol and a Gaussian width of 1 Å was applied every 500 ps with a bias factor of 15. The WTMD simulations were conducted over 115 ns for each system and convergence of the FESs was calculated by tracking the evolution of the FESs over each additional 5 ns. FESs for all systems were found to have converged to within 1 kcal/mol at the end of the 115 ns simulation (Supporting Information Figure S2).

3. Results and Discussion

3.1 System Properties.

Table 1 lists the systems that are considered in this study along with the observed densities, radii of gyration and self-diffusivity coefficients for the solvent atoms with the numbers in parenthesis corresponding to experimentally observed values. The densities calculated from our simulated pure IL systems are found to be in excellent agreement with experimentally measured pure IL densities (*i.e.*, within 3%).^{45, 46} In addition to the density, the radii of gyration was calculated as it provides an estimate of the compactness of the molecule and, as expected, the values increase as the alkyl chain increases. The self-diffusivity coefficients were evaluated from NVE simulations using the Einstein's relation, which relates the mean square displacements (MSD) to the diffusion coefficients. The calculated MSD for EMIM OAc compares well with available experimental values, and reproduces the experimentally observed difference between the cation and anion diffusion coefficients (*i.e.*, the anion diffuses ~0.9 times that of the cation).⁴⁷

Table 1: System Parameters[†].

System		System Densities (gm/cc, 300 K)	Radius of gyration of cation (Å)	Solvent Diffusion (cm ² /s)		Wt % Sugar
				Cation	Anion	
Control	1G	1.00	-	Water		0.13
	2G	1.00	-	6.09 x 10 ⁻⁵	6.49 x 10 ⁻⁵	0.25
EMIM	1G	1.13 (1.12 ⁴⁸)	2.59 ± 0.1	1.69 (1.40 ⁴⁷) x 10 ⁻⁷	1.57 x 10 ⁻⁷	0.13
	2G	1.13 (1.12 ⁴⁸)	2.59 ± 0.1	1.76 (1.53 ⁴⁷) x 10 ⁻⁷	1.34 x 10 ⁻⁷	0.25
BMIM	1G	1.08 (1.05 ⁴⁹)	3.08 ± 0.1	1.41 x 10 ⁻⁷	1.1 x 10 ⁻⁷	0.13
	2G	1.08 (1.05 ⁴⁹)	3.08 ± 0.1	1.43 x 10 ⁻⁷	1.24 x 10 ⁻⁷	0.25
OMIM	1G	1.01	4.07 ± 0.3	3.55 x 10 ⁻⁷	2.14 x 10 ⁻⁷	0.15
	2G	1.01	4.04 ± 0.3	3.17 x 10 ⁻⁷	1.8 x 10 ⁻⁷	0.28

[†]The values in parentheses are experimentally observed values.

The solvation of IL-cellulose systems at the molecular level has been characterized *via* radial distribution functions (RDFs), conformation of the ω dihedral (*i.e.*, trans-gauche, gauche-trans and gauche-gauche) and the ϕ - ψ plots for the glycosidic bond.^{23, 25, 50} The following sections discuss and compare each of these characteristics, in detail, from the context of EMIM OAc, BMIM OAc and OMIM OAc solvation of glucose and cellobiose with respect to an aqueous environment.

3.2 Solvent-Solvent and Solvent-Solute Structure

RDFs are central to understanding solvation structure and are therefore used to evaluate the polar interactions between cation (alkylimidazolium C4) and anion (OAc C2) observed over the 100 ns unbiased trajectories (Figure 2).⁵⁰ In all 3 IL systems there is a distinct double peak at 3.8 Å and 5.7 Å in the cation-anion RDF, which is consistent with previously reported observations for EMIM OAc.^{25, 26} The coordination number for the first solvation shell is calculated to be around

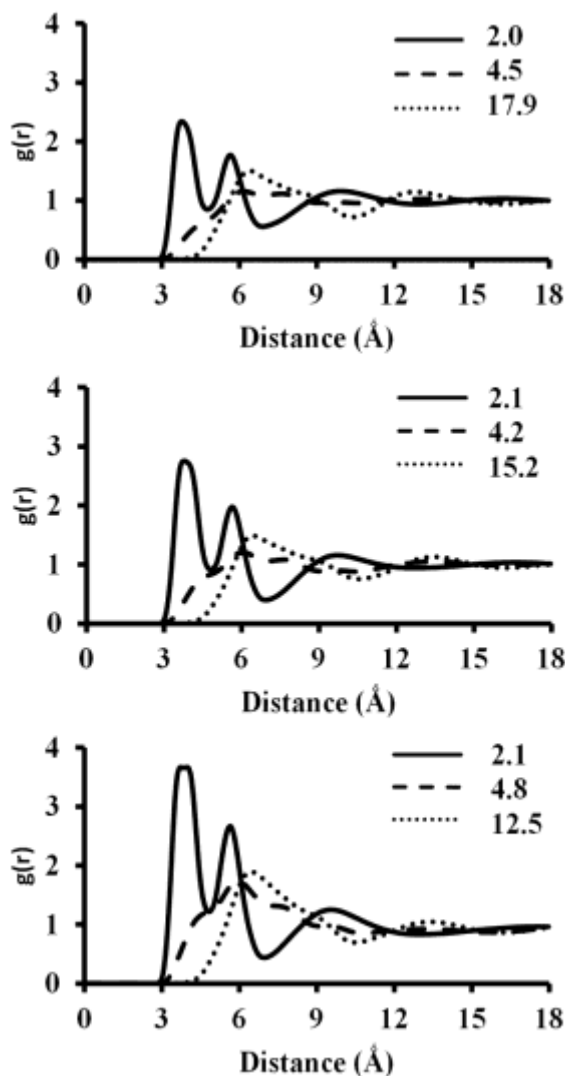


Figure 2 RDFs depicting the polar interactions between the cation and anion in the presence of glucose. The cation is represented by the C4 atom in the alkylimidazolium while the anion is represented by the C2 in OAc. The Cation-anion (solid line), cation-cation (dashed line), and anion-anion (dotted line) interactions are presented for EMIM OAc (top), BMIM OAc (middle), and OMIM OAc (bottom). The coordination numbers are reported in the inset.

2, indicating that on average 2 anions can be found relatively close to the alkylimidazolium (*i.e.*, $\sim 3 \text{ \AA}$ to $\sim 4.8 \text{ \AA}$) and the presence of an ordered repeating of cation-anion solvation shells. The cation-cation and anion-anion interactions are characterized by a broad first peak with the cation-cation possessing a maximum around 6 \AA and shoulder features that indicate the 1st, 2nd, and 3rd solvation shells while the anion-anion has a maximum around 6.4 \AA , a clear 1st solvation shell, and shoulders that indicate subsequent solvation shells. The reported coordination numbers for the cation-anion (3 \AA to $\sim 4.8 \text{ \AA}$) and cation-cation (3 \AA to $\sim 7 \text{ \AA}$) interactions is similar for the 3 ILs at 2 and ~ 4.5 , respectively. The cutoff value of $\sim 7 \text{ \AA}$ for the cation-cation interaction indicates the combination of the 1st and 2nd solvation shells with the 1st solvation shell being depicted by the shoulder feature at around 4.5 \AA . The coordination number for the anion-anion interaction was taken between 3 \AA and 10.5 \AA , and similar to the cation-cation interaction, encompasses the 1st, 2nd, and possible 3rd solvation shells. It is interesting to note that the increasing size of the cation's alkyl tail length has no significant impact on the overall solvent structure. It is noted that the observed decrease in the anion-anion coordination number as the alkyl tail length increases is due to the reduced number of ion pairs. The RDFs for the 2G system are nearly indistinguishable from the 1G system and are therefore not shown.

The presence of hydroxyl groups on both the solute (*i.e.*, 1G and 2G) and the IL's anion result in characteristic sugar-anion and sugar-cation interactions as illustrated in Figure 3 for the 1G and 2G systems. The RDFs consider the hydroxyl oxygens on the sugar (O2, O3 and O6); the C4 carbon on the cation for the sugar-cation interactions, and the C2 carboxylic carbon on the anion for sugar anion interactions.⁵⁰ The location of the first peak for the sugar-anion interaction occurs at 2.6 \AA for all the 3 ILs indicating that the sugars are first solvated by the acetate anions and that

the increasing imidazolium cation chain length does not impact acetate solvation of the sugar's hydroxyl groups. The first sugar-cation peak occurs between 3.3 Å and 3.5 Å for all the cations indicating that the second solvation shell contains primarily the cation. Further solvation shells are not as well defined but appear to alternate between the anions and cations, in line with the current hypothesis of IL structure and solvation characteristics of sugars.⁵⁰

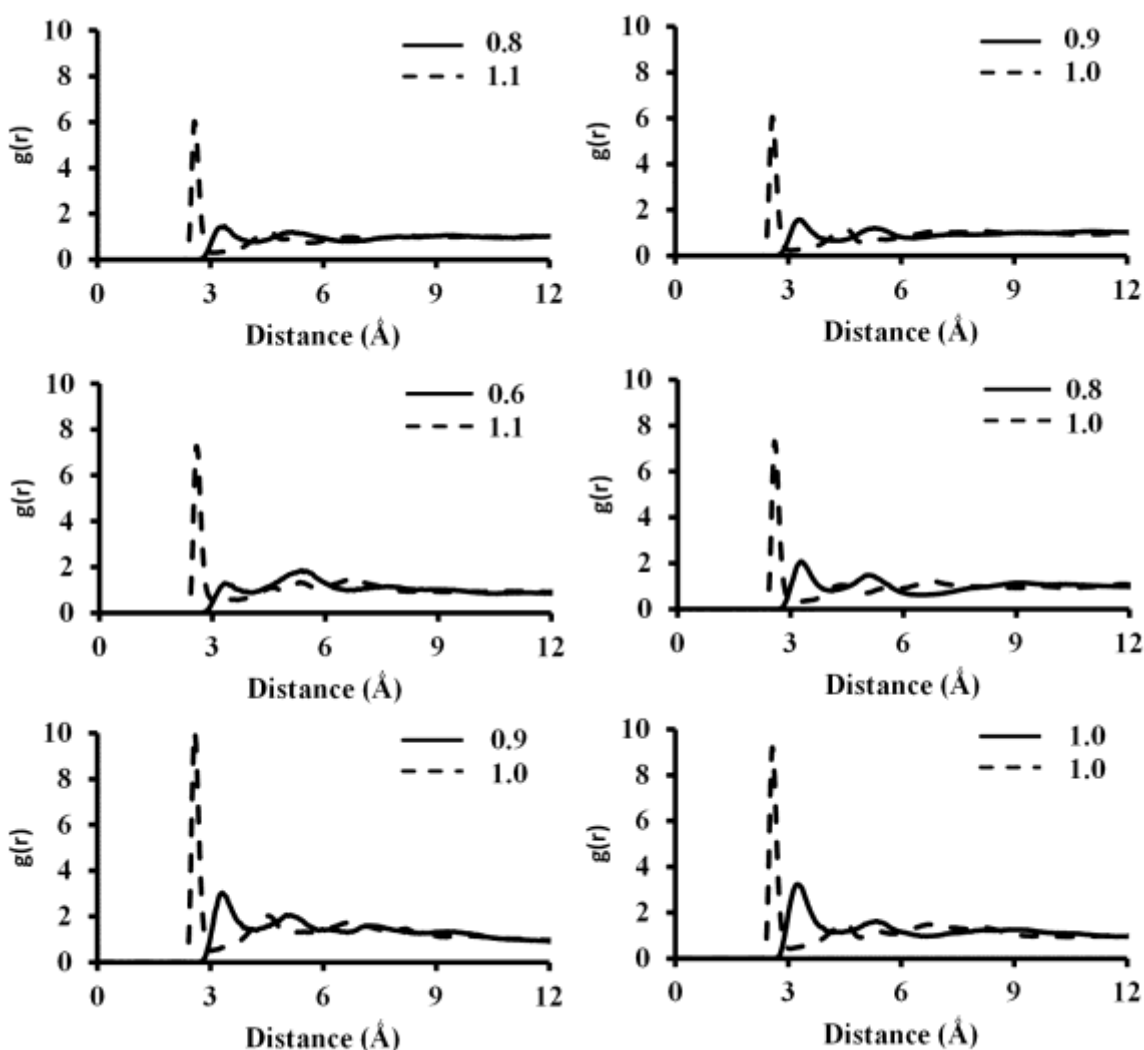


Figure 3 RDFs depicting the solvent-solute interactions. The sugar-cation (solid line), and sugar-anion (dashed line) interactions are presented for EMIM OAc (top), BMIM OAc (middle), and OMIM OAc (bottom) for the glucose (left) and cellobiose (right) systems. The coordination numbers are reported in the inset.

3.3 The conformation of the ω dihedral

It has been observed in the literature that the presence of ILs impacts the ω dihedral (O6-C6-C5-O5) conformation for the hydroxymethyl group in oligosaccharides.²²⁻²⁵ In water, the ω dihedral is observed to equally sample the gauche-gauche (GG; $\omega = \sim -60^\circ$) and the gauche-trans (GT; $\omega = \sim 60^\circ$) conformations with a minor amount of conformations observed in the trans-gauche (TG; $\omega = \sim 180^\circ$). However, in the presence of ILs the distribution of the ω dihedral angle is found to shift predominantly towards the GT conformation. These observations are also seen in our simulations of 1G in ILs, where the ω dihedral distribution is found to shift towards the GT conformation irrespective of the cation's alkyl chain length, Figure 4. In recent studies, this shift in the conformational distribution of the ω dihedral in ILs has been linked to the formation of an intramolecular hydrogen bond between O2 and O6 of adjacent saccharide rings.^{22, 23} However, we observe a similar shift in the ω dihedral distributions for our 1G in ILs simulations, which doesn't involve the O2-O6 intramolecular H-bond. This observation leads us to believe that the very presence of the IL plays a role in impacting the ω dihedral distribution. Clearly, a new hypothesis must be presented that adequately describes the role of ILs on the shifted ω dihedral distribution and is valid for glucose, cellobiose, and larger oligosaccharides.

The potentials of mean force (PMFs) describing the rotation around the ω dihedral

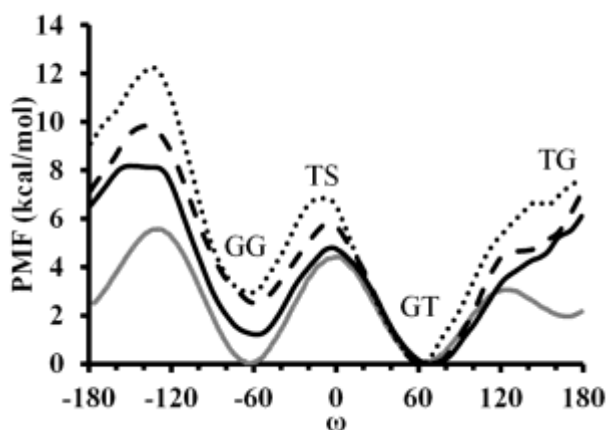


Figure 4 PMFs for the rotation of the ω dihedral (C5-O5-C6-O6) in EMIM OAc (solid black), BMIM OAc (black dashed), OMIM OAc (black dotted), and water (solid grey). The GG, GT and TG wells have been indicated according to their corresponding ω values in addition to the transition state (TS) between GG and GT.

in glucose (Figure 4) clearly indicate that in water (grey line) the wells for the GT ($\sim 60^\circ$), GG ($\sim 60^\circ$) conformations are thermodynamically equivalent, and are separated by a barrier of 4 kcal/mole located at 0° , in agreement with previously published work.²⁵ Analysis of the transition state (TS) region between the GG and GT wells indicates that this barrier is caused by repulsive interactions between the electro-negative hydroxymethyl oxygen (O6) atom and the ring oxygen (O5) atom. The unfavorable interaction arises because the two groups are in the same plane and reside in close proximity (~ 2.7 Å). In the presence of ILs, the GG conformation is found to be less stable as compared to the GT conformation. Furthermore, it is observed that the GG well becomes increasingly more unstable as the cation's tail length increases (EMIM OAc: 1.2 kcal/mol, BMIM OAc: 2.5 kcal/mol and EMIM OAc: 3.0 kcal/mol). These results indicate that the cation's alkyl tail interactions play a role in determining the stability of GG and GT wells thereby shifting the orientation of the ω dihedral.

To evaluate the role of the cation's alkyl tail, iso-surface plots for the volumetric occupancy around glucose for the 3 different ILs in the destabilized GG well and the stable GT well were created (Figure 5). In the presence of ILs, it is observed that the electronegative nature of the ring oxygen attracts the positively charged imidazolium ring of the cation (note the green iso-surface in front of the sugar ring oxygen in Figure 5). In the GG well, this interaction places the cation's alkyl tail in close proximity to the space occupied by the sugar's hydroxymethyl group. As the tail length increases, the unfavorable hydrophobic-hydrophilic interaction increases, resulting in the destabilization of the GG well. This interaction also explains the progressively higher energy for the TS region ($\omega \sim 0^\circ$) as the cation's alkyl tail length increases (Supporting Information Figure S3). In the GT ($\omega \sim 60^\circ$) well, the conformation of the hydroxymethyl group places it

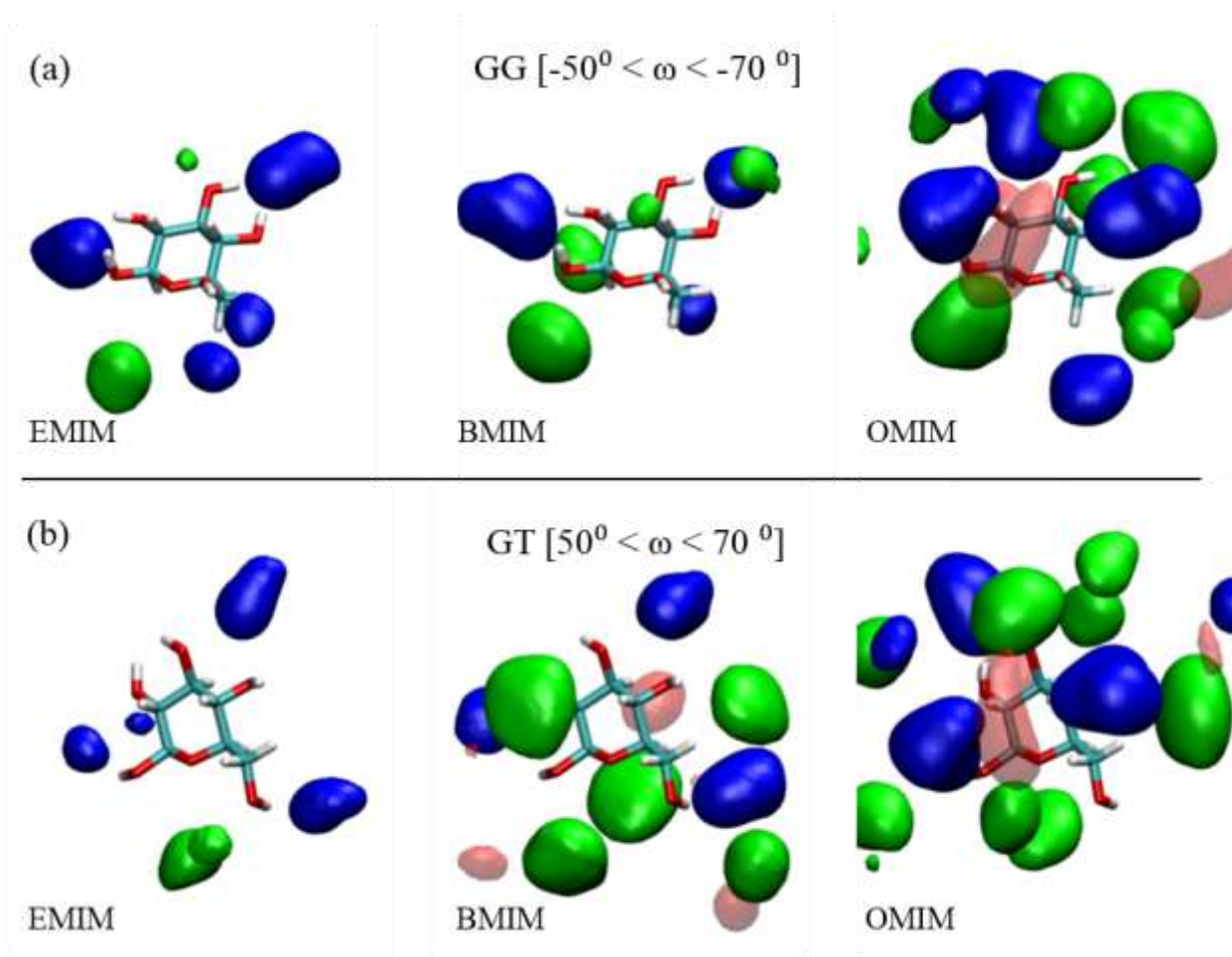


Figure 5 Iso-surface plots based on volumetric occupancy of acetates (Blue), Imidazolium ring (Green) and Cation Tail (Red Transparent) in the GG well (a) and GT well (b) for EMIM OAc (left) BMIM OAc (center) and OMIM OAc (right).

farther away from the sugar ring's oxygen, thus enabling the accommodation of the cation's alkyl tail. This elimination of unfavorable contacts in the GT well results in a conformation of the hydroxymethyl group that is stable for all 3 ILs, irrespective of the cation's alkyl tail length.

3.4 Free energy surfaces for rotation around the glycosidic bond (ϕ - ψ plots) The relative orientation of the carbohydrate rings in any oligosaccharide is dictated by the specific value of the ϕ (O5-C1-O4-C4) and ψ (C1-O4-C4-C5) dihedral angles. In the case of cellobiose, the orientation of the rings impacts the glycosidic bond's accessibility to the solvent, which is particularly relevant for the hydrolysis of the glycosidic bond. In our MD simulations, the

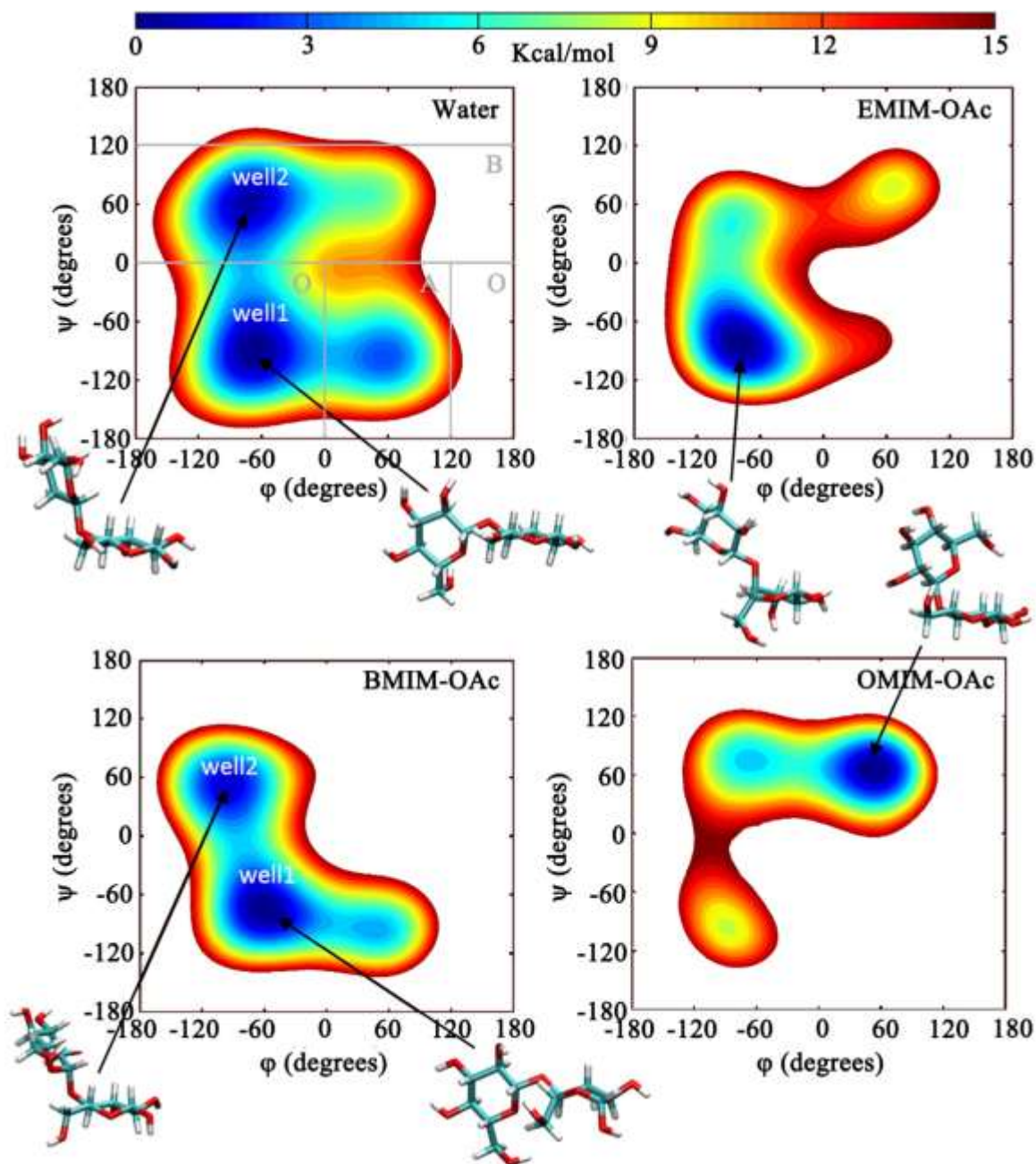


Figure 6 Free energy surfaces obtained from Metadynamics simulations of 2G in water (top left) EMIM OAc (top right), BMIM OAc (bottom left) and OMIM OAc (bottom right). The aligned structures of 2G corresponding to each well are shown in licorice representation. In the case of Water and BMIM OAc, Well1 indicates the lower energy well and Well2 is higher by 0.5 kcal/mol for Water and 1.2 kcal/mol for BMIM OAc.

preferred orientation of the cellobiose glycosidic bond in ILs is observed to be shifted in the presence of ILs. While this orientational shift of the glycosidic bond in oligosaccharides in the presence of ILs has been observed in earlier studies by Liu *et al.*²⁵ and Mostofian *et al.*²² the

energetics that drive the orientational shift have not yet been explored. Unlike the ω dihedral, which involved biased sampling along a single coordinate, sampling the ϕ - ψ involves sampling across 2 dimensions and the generation of a 2-D PMF. The ϕ - ψ conformational space of cellobiose in water has been previously explored using replica exchange MD and the free energy surface (FES) elucidated using umbrella sampling.^{51, 52} In these previous works it was found that cellobiose prefers 3 distinct regions of the ϕ - ψ plot labeled in Figure 6 as O, A and B in increasing order of probability.

Figure 6 depicts the well tempered metadynamics (WTMD) derived FESs that describe the conformational ϕ - ψ energy landscape for cellobiose (2G) in water and the 3 ILs along with the sugar conformations in the observed wells. The FES and the low energy wells observed in the case of water are consistent with existing literature and indicate that the lowest energy basin is the O basin followed by the B and A basins.^{22, 51, 52} It is observed that the lowest energy wells in the B and A basins are ~ 0.5 kcal/mol and ~ 3.5 kcal/mol higher than the lowest energy well in the O basin, respectively. The ϕ - ψ energy landscape for 2G in EMIM OAc and OMIM OAc is characterized by a single low energy well while BMIM OAc has 2 low energy wells. In the case of EMIM OAc, the energy minimum is found to be in the O region with a relatively flat plateau in the B region that is ~ 6 kcal/mol higher in energy than the O region. The OMIM OAc energy landscape is characterized by a single well and a ~ 5 kcal/mol higher plateau that corresponds to the B region. BMIM OAc is observed to have 2 wells one each in the O and B regions, similar to the water case, and a plateau in the A region that is ~ 5 kcal higher in energy. In two recent studies involving oligosaccharide solvation in BMIM chloride and BMIM OAc, it was found that the regions of stable conformation for the glycosidic bond were predominantly in the O and B regions, which is in good agreement with our results.^{9, 27}

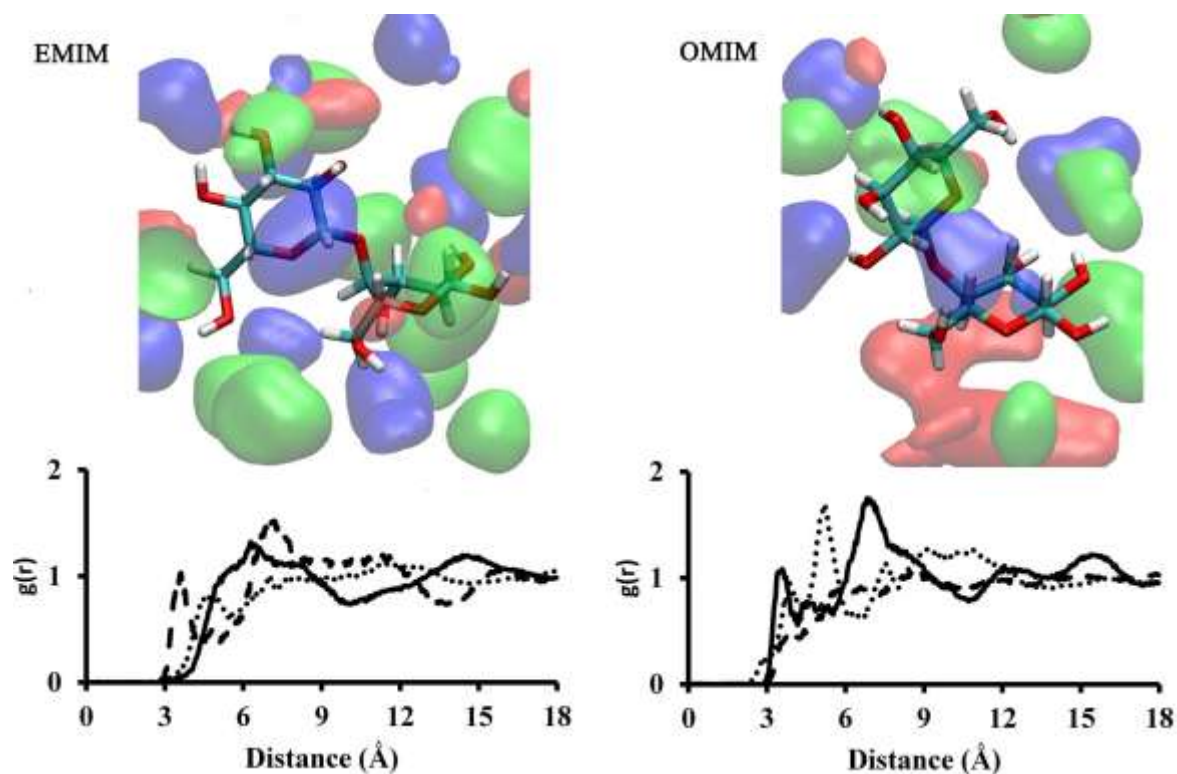


Figure 7 Iso-surface plots based on volumetric occupancy (Top) calculated from the conformations observed in the EMIM OAc (left) and OMIM OAc (Right) ϕ - ψ wells. The acetates are represented in transparent Blue, Imidazolium ring in transparent Green and Cation Tail in transparent Red. The interactions of the Glycosidic Oxygen with the imidazolium ring (solid line), alkyl tail (dashed line) and the acetates (dotted line) indicated by RDFs (Bottom).

To describe the orientation of the glycosidic bond and evaluate the specific molecular interactions in these wells, all conformations within 3 kcal/mol of the lowest point in the well were analyzed.

The interactions of the glycosidic oxygen and ring oxygens with the solvent (acetate, imidazolium ring and alkyl tail) were evaluated using RDFs and iso-surface plots based on volumetric occupancy. These iso-surface plots and the glycosidic oxygen RDFs for the single wells of EMIM OAc and OMIM OAc are depicted in Figure 7. In EMIM OAc, the glycosidic oxygen is observed to interact with the cation's alkyl tails (~ 3 Å) and with the imidazolium ring at (~ 6 Å), while the anion interactions appear to be disordered. The ring oxygens of the cellobiose primarily interact with the cation imidazolium ring and the alkyl tails (Supporting

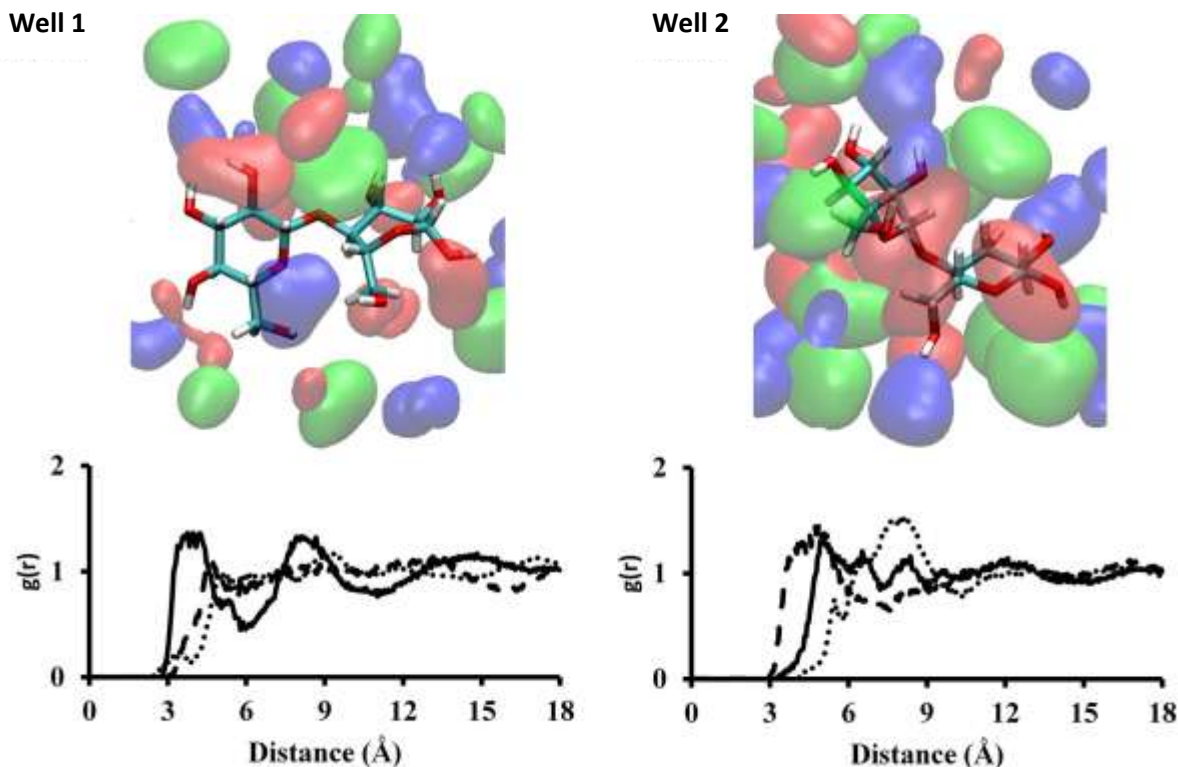


Figure 8 Iso-surface plots based on volumetric occupancy calculated from the conformations observed in the BMIM OAc ϕ - ψ Well 1 (left) and Well 2 (right). The acetates are represented in transparent Blue, Imidazolium ring in transparent Green and Cation Tail in transparent Red. The interactions of the Glycosidic Oxygen with the imidazolium ring (solid line), alkyl tail (dashed line) and the acetates (dotted line) indicated by RDFs (Bottom).

Information Figure S4). The ϕ - ψ energy minima for OMIM OAc is found to orient the glycosidic bond into an alternative conformation than that seen in EMIM OAc, which allows the glycosidic oxygen to have increased interactions with the imidazolium ring (~ 3 Å). This particular RDF also indicates the repeating cation-anion solvation characteristics with the next solvation shell out from the imidazolium ring being occupied by acetates (~ 6 Å) and then followed again by the imidazolium ring (~ 7 Å). Unlike EMIM OAc the ring oxygens of cellobiose in OMIM OAc primarily interact with the alkyl tail (Supporting Information Figure S4).

The orientation of the glycosidic bond and its solvent interactions in the two BMIM OAc wells are compared in Figure 8. In well 1, the glycosidic bond is more exposed to the solvent as compared to well 2, and is characterized by close interactions with the cation's imidazolium ring

(~3-4 Å). Contrastingly, well 2, is characterized by the glycosidic oxygen predominantly interacting with the cation's alkyl tail (~3-5 Å), followed by interactions with the imidazolium ring (~5 Å). The higher free energy associated with well 2 is hypothesized to be attributed to the conformational rigidity (or loss of entropy) due to the presence of the relatively larger alkyl tails around the glycosidic bond. Supporting this hypothesis is the observation that the ring oxygens in this well interact closely with the cation's alkyl tail and the imidazolium ring (Supporting Information Figure S5).

4. Conclusions

A systematic approach to understanding the impact of the cation's alkyl chain length on the solvation of 1G and 2G has been undertaken *via* fully atomistic molecular dynamics simulations. The observations of structural and conformational properties in this study are consistent with existing literature and reveal that the increasing alkyl tail length of the cation does not impact the acetate solvation of the hydroxyl groups of 1G and 2G. It is apparent from the MD simulations that the presence of ILs significantly restricts the conformational sampling of 1G and 2G. This may be attributed to the inherently viscous nature of the ILs, which extends the simulation timescales required to observe adequate conformational sampling. While the intramolecular H-bonding in oligosaccharides was hypothesized to be responsible for the skewed distributions of the ω dihedral, observations of similar skewed distributions is found for the 1G systems, which do not possess the purported molecular H-bonding. It is found that the cation's hydrophobic alkyl tail interactions with the sugar's hydrophilic hydroxymethyl group is the main driving force for the observed shifting in the ω dihedral.

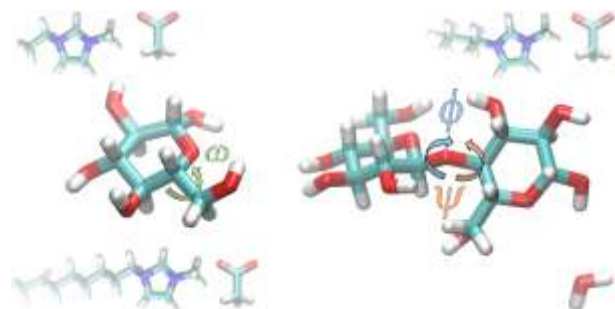
The energetics governing the rotation of the hydroxymethyl group in glucose, measured *via* the ω dihedral, were elucidated through the calculation of the potential of mean force for rotation about the ω dihedral in water as well as the 3 ILs. It was found that the GG and GT conformations are thermodynamically equivalent in water, but in ILs it is observed that the GT conformation is more stable than the GG conformation. The interaction of the imidazolium ring with the oxygen of the glucose ring causes the placement of the alkyl tail to reside close to the hydroxymethyl group in the GG conformation. This unfavorable interaction also explains the increasing instability of the GG conformation with increasing alkyl tail length. The free energy surface governing the orientation of the glycosidic bond has also been explored for cellobiose in water and the 3 ILs, and indicates a single well for EMIM OAc and OMIM OAc and double wells for BMIM OAc. The double wells in the case of BMIM OAc are in general agreement with the regions of stable conformation observed in previous reports of BMIM chloride and BMIM OAc. The volumetric occupancy maps and RDFs for the conformations in the wells indicate specific interactions that stabilize cellobiose in the corresponding wells and indicate that the character of the cation is the main driving force for the shifting in observed dihedrals about the glycosidic bond.

5. Acknowledgements

The authors would like to acknowledge financial support from the National Science Foundation under the CBET award no. 1337044. The authors would also like to acknowledge support from the High Performance Computing department of the Colorado School of Mines for facilitating the use of supercomputing resources. Contributions from Mr. David Granum, Colorado Center for Biorefining and Biofuels (C2B2) REU student Ms. Samantha Sherman, and CBET REU student Mr. Adam Smith are also acknowledged.

Supporting Information. Convergence of PMF calculations using Umbrella Sampling, Convergence of Well-Tempered Metadynamics derived FES for ϕ - ψ dihedrals, Barrier at the TS for the ω dihedral for the 3 ILs and Interactions of the cellobiose ring oxygens with the solvent.

Table of Contents Graphic:



References

1. Swatloski, R. P., Spear, S. K., Holbrey, J. D., and Rogers, R. D. (2002) Dissolution of Cellulose with Ionic Liquids, *Journal of the American Chemical Society* 124, 4974-4975.
2. Zhu, S., Wu, Y., Chen, Q., Yu, Z., Wang, C., Jin, S., Ding, Y., and Wu, G. (2006) Dissolution of cellulose with ionic liquids and its application: a mini-review, *Green Chemistry* 8, 325-327.
3. Tadesse, H., and Luque, R. (2011) Advances on biomass pretreatment using ionic liquids: An overview, *Energy & Environmental Science* 4, 3913-3929.
4. Welton, T. (1999) Room-Temperature Ionic Liquids. Solvents for Synthesis and Catalysis, *Chemical Reviews* 99, 2071-2084.
5. Song, J., Fan, H., Ma, J., and Han, B. (2013) Conversion of glucose and cellulose into value-added products in water and ionic liquids, *Green Chemistry* 15, 2619-2635.
6. Nanayakkara, S., Patti, A. F., and Saito, K. (2014) Lignin Depolymerization with Phenol via Redistribution Mechanism in Ionic Liquids, *ACS Sustainable Chemistry & Engineering* 2, 2159-2164.
7. Lan, W., Liu, C.-F., and Sun, R.-C. (2011) Fractionation of Bagasse into Cellulose, Hemicelluloses, and Lignin with Ionic Liquid Treatment Followed by Alkaline Extraction, *Journal of Agricultural and Food Chemistry* 59, 8691-8701.
8. Shi, J., Balamurugan, K., Parthasarathi, R., Sathitsuksanoh, N., Zhang, S., Stavila, V., Subramanian, V., Simmons, B. A., and Singh, S. (2014) Understanding the role of water during ionic liquid pretreatment of lignocellulose: co-solvent or anti-solvent?, *Green Chemistry* 16, 3830-3840.
9. Xu, J., Wu, B., Hu, L., Wu, Z., Xu, N., Dai, B., and He, J. (2015) Enzymatic in situ saccharification of lignocellulose in a compatible ionic liquid-cellulase system, *Chemical Engineering Journal* 267, 163-169.
10. Ren, H., Zhou, Y., and Liu, L. (2013) Selective conversion of cellulose to levulinic acid via microwave-assisted synthesis in ionic liquids, *Bioresource technology* 129, 616-619.
11. Zhao, H., Holladay, J. E., Brown, H., and Zhang, Z. C. (2007) Metal chlorides in ionic liquid solvents convert sugars to 5-hydroxymethylfurfural, *Science* 316, 1597-1600.
12. Yong, G., Zhang, Y., and Ying, J. Y. (2008) Efficient Catalytic System for the Selective Production of 5-Hydroxymethylfurfural from Glucose and Fructose, *Angewandte Chemie International Edition* 47, 9345-9348.
13. Kim, B., Jeong, J., Lee, D., Kim, S., Yoon, H.-J., Lee, Y.-S., and Cho, J. K. (2011) Direct transformation of cellulose into 5-hydroxymethyl-2-furfural using a combination of metal chlorides in imidazolium ionic liquid, *Green Chemistry* 13, 1503-1506.
14. Ding, Z.-D., Shi, J.-C., Xiao, J.-J., Gu, W.-X., Zheng, C.-G., and Wang, H.-J. (2012) Catalytic conversion of cellulose to 5-hydroxymethyl furfural using acidic ionic liquids and co-catalyst, *Carbohydrate Polymers* 90, 792-798.
15. Chatel, G., and Rogers, R. D. (2013) Review: Oxidation of Lignin Using Ionic Liquids—An Innovative Strategy To Produce Renewable Chemicals, *ACS Sustainable Chemistry & Engineering* 2, 322-339.
16. Socha, A. M., Parthasarathi, R., Shi, J., Pattathil, S., Whyte, D., Bergeron, M., George, A., Tran, K., Stavila, V., and Venkatachalam, S. (2014) Efficient biomass pretreatment using ionic liquids derived from lignin and hemicellulose, *Proceedings of the National Academy of Sciences* 111, E3587-E3595.

17. Uppugundla, N., da Costa Sousa, L., Chundawat, S. P. S., Yu, X., Simmons, B., Singh, S., Gao, X., Kumar, R., Wyman, C. E., and Dale, B. E. (2014) A comparative study of ethanol production using dilute acid, ionic liquid and AFEX™ pretreated corn stover, *Biotechnology for biofuels* 7, 72.
18. Yan, N., Zhao, C., Luo, C., Dyson, P. J., Liu, H., and Kou, Y. (2006) One-Step Conversion of Cellobiose to C6-Alcohols Using a Ruthenium Nanocluster Catalyst, *Journal of the American Chemical Society* 128, 8714-8715.
19. Wahlstrom, R. M., and Surnakki, A. (2015) Enzymatic hydrolysis of lignocellulosic polysaccharides in the presence of ionic liquids, *Green Chemistry*.
20. Lee, S. H., Doherty, T. V., Linhardt, R. J., and Dordick, J. S. (2009) Ionic liquid-mediated selective extraction of lignin from wood leading to enhanced enzymatic cellulose hydrolysis, *Biotechnology and Bioengineering* 102, 1368-1376.
21. Fu, D., Mazza, G., and Tamaki, Y. (2010) Lignin Extraction from Straw by Ionic Liquids and Enzymatic Hydrolysis of the Cellulosic Residues, *Journal of Agricultural and Food Chemistry* 58, 2915-2922.
22. Mostofian, B., Cheng, X., and Smith, J. C. (2014) Replica-Exchange Molecular Dynamics Simulations of Cellulose Solvated in Water and in the Ionic Liquid 1-Butyl-3-Methylimidazolium Chloride, *The Journal of Physical Chemistry B* 118, 11037-11049.
23. Liu, H., Cheng, G., Kent, M., Stavila, V., Simmons, B. A., Sale, K. L., and Singh, S. (2012) Simulations Reveal Conformational Changes of Methylhydroxyl Groups during Dissolution of Cellulose I β in Ionic Liquid 1-Ethyl-3-methylimidazolium Acetate, *The Journal of Physical Chemistry B* 116, 8131-8138.
24. Bellesia, G., Chundawat, S. P. S., Langan, P., Dale, B. E., and Gnanakaran, S. (2011) Probing the Early Events Associated with Liquid Ammonia Pretreatment of Native Crystalline Cellulose, *The Journal of Physical Chemistry B* 115, 9782-9788.
25. Liu, H., Sale, K. L., Holmes, B. M., Simmons, B. A., and Singh, S. (2010) Understanding the Interactions of Cellulose with Ionic Liquids: A Molecular Dynamics Study, *The Journal of Physical Chemistry B* 114, 4293-4301.
26. Niazi, A. A., Rabideau, B. D., and Ismail, A. E. (2013) Effects of Water Concentration on the Structural and Diffusion Properties of Imidazolium-Based Ionic Liquid–Water Mixtures, *The Journal of Physical Chemistry B* 117, 1378-1388.
27. Velioglu, S., Yao, X., Devémy, J., Ahunbay, M. G., Tantekin-Ersolmaz, S. B., Dequidt, A., Costa Gomes, M. F., and Pádua, A. A. H. (2014) Solvation of a Cellulose Microfibril in Imidazolium Acetate Ionic Liquids: Effect of a Cosolvent, *The Journal of Physical Chemistry B*.
28. Vitz, J., Erdmenger, T., Haensch, C., and Schubert, U. S. (2009) Extended dissolution studies of cellulose in imidazolium based ionic liquids, *Green Chemistry* 11, 417-424.
29. D.A. Case, T. A. D., T.E. Cheatham, III, C.L. Simmerling, J. Wang, R.E. Duke, R., Luo, R. C. W., W. Zhang, K.M. Merz, B. Roberts, B. Wang, S. Hayik, A. Roitberg,, G. Seabra, I. K., K.F. Wong, F. Paesani, J. Vanicek, J. Liu, X. Wu, S.R. Brozell,, T. Steinbrecher, H. G., Q. Cai, X. Ye, J. Wang, M.-J. Hsieh, G. Cui, D.R. Roe, D.H., Mathews, M. G. S., C. Sagui, V. Babin, T. Luchko, S. Gusarov, A. Kovalenko, and, and Kollman, P. A. (2010) AMBER 11, University of California, San Francisco.
30. Bonomi, M., Branduardi, D., Bussi, G., Camilloni, C., Provasi, D., Raiteri, P., Donadio, D., Marinelli, F., Pietrucci, F., Broglia, R. A., and Parrinello, M. (2009) PLUMED: A

- portable plugin for free-energy calculations with molecular dynamics, *Computer Physics Communications* 180, 1961-1972.
31. Sambasivarao, S. V., and Acevedo, O. (2009) Development of OPLS-AA Force Field Parameters for 68 Unique Ionic Liquids, *Journal of Chemical Theory and Computation* 5, 1038-1050.
 32. Kirschner, K. N., Yongye, A. B., Tschampel, S. M., González-Outeiriño, J., Daniels, C. R., Foley, B. L., and Woods, R. J. (2008) GLYCAM06: A generalizable biomolecular force field. Carbohydrates, *Journal of Computational Chemistry* 29, 622-655.
 33. Jorgensen, W. L., Chandrasekhar, J., Madura, J. D., Impey, R. W., and Klein, M. L. (1983) Comparison of simple potential functions for simulating liquid water, *The Journal of Chemical Physics* 79, 926-935.
 34. Martinez, L., Andrade, R., Birgin, E. G., and Martinez, J. M. (2009) PACKMOL: A Package for Building Initial Configurations for Molecular Dynamics Simulations, *Journal of Computational Chemistry* 30, 2157-2164.
 35. Ryckaert, J.-P., Ciccotti, G., and Berendsen, H. (1977) Numerical integration of the cartesian equations of motion of a system with constraints: molecular dynamics of n-alkanes, *Journal of Computational Physics* 23, 327-341.
 36. Kirschner, K. N., and Woods, R. J. (2001) Solvent interactions determine carbohydrate conformation, *Proceedings of the National Academy of Sciences* 98, 10541-10545.
 37. Shankar, K., Djamal, B., Robert, H. S., Peter, A. K., and John, M. R. (1992) The weighted histogram analysis method for free-energy calculations on biomolecules. I: The method, *J. Comput. Chem.* 13, 1011-1021.
 38. Roux, B. (1995) The calculation of the potential of mean force using computer simulations, *Computer Physics Communications* 91, 275-282.
 39. Grossfield, A. WHAM: the weighted histogram analysis method 2.0.6 ed.
 40. Bussi, G., Gervasio, F. L., Laio, A., and Parrinello, M. (2006) Free-energy landscape for beta hairpin folding from combined parallel tempering and metadynamics, *Journal of the American Chemical Society* 128, 13435-13441.
 41. Biarnes, X., Ardevol, A., Planas, A., Rovira, C., Laio, A., and Parrinello, M. (2007) The conformational free energy landscape of beta-D-glucopyranose. implications for substrate preactivation in beta-glucoside hydrolases, *Journal of the American Chemical Society* 129, 10686-10693.
 42. Jarin, Z., and Pfaendtner, J. (2014) Ionic Liquids Can Selectively Change the Conformational Free-Energy Landscape of Sugar Rings, *Journal of Chemical Theory and Computation* 10, 507-510.
 43. Gervasio, F. L., Laio, A., and Parrinello, M. (2005) Flexible docking in solution using metadynamics, *Journal of the American Chemical Society* 127, 2600-2607.
 44. Barducci, A., Bussi, G., and Parrinello, M. (2008) Well-tempered metadynamics: A smoothly converging and tunable free-energy method, *Physical Review Letters* 100.
 45. Zhang, S., Sun, N., He, X., Lu, X., and Zhang, X. (2006) Physical Properties of Ionic Liquids: Database and Evaluation, *Journal of Physical and Chemical Reference Data* 35, 1475-1517.
 46. Tariq, M., Forte, P. A. S., Gomes, M. F. C., Lopes, J. N. C., and Rebelo, L. P. N. (2009) Densities and refractive indices of imidazolium- and phosphonium-based ionic liquids: Effect of temperature, alkyl chain length, and anion, *The Journal of Chemical Thermodynamics* 41, 790-798.

47. Ries, M. E., Radhi, A., Keating, A. S., Parker, O., and Budtova, T. (2014) Diffusion of 1-Ethyl-3-methyl-imidazolium Acetate in Glucose, Cellobiose, and Cellulose Solutions, *Biomacromolecules* 15, 609-617.
48. Hall, C. A., Le, K. A., Rudaz, C., Radhi, A., Lovell, C. S., Damion, R. A., Budtova, T., and Ries, M. E. (2012) Macroscopic and Microscopic Study of 1-Ethyl-3-methyl-imidazolium Acetate–Water Mixtures, *The Journal of Physical Chemistry B* 116, 12810-12818.
49. Almeida, H. F. D., Passos, H., Lopes-da-Silva, J. A., Fernandes, A. M., Freire, M. G., and Coutinho, J. A. P. (2012) Thermophysical Properties of Five Acetate-Based Ionic Liquids, *Journal of Chemical & Engineering Data* 57, 3005-3013.
50. Liu, H., Sale, K. L., Simmons, B. A., and Singh, S. (2011) Molecular Dynamics Study of Polysaccharides in Binary Solvent Mixtures of an Ionic Liquid and Water, *The Journal of Physical Chemistry B* 115, 10251-10258.
51. Perić-Hassler, L., Hansen, H. S., Baron, R., and Hünenberger, P. H. (2010) Conformational properties of glucose-based disaccharides investigated using molecular dynamics simulations with local elevation umbrella sampling, *Carbohydrate Research* 345, 1781-1801.
52. Shen, T., Langan, P., French, A. D., Johnson, G. P., and Gnanakaran, S. (2009) Conformational Flexibility of Soluble Cellulose Oligomers: Chain Length and Temperature Dependence, *Journal of the American Chemical Society* 131, 14786-14794.